J Therm Anal Calorim (2018) 131:81–88
https://doi.org/10.1007/s10973-017-6556-1

Preparation and thermal performance of *n*-octadecane/expanded graphite composite phase-change materials for thermal management

Yongpeng Xia[1,2] · Weiwei Cui[1,2] · Huanzhi Zhang[1,2,3] · Yongjin Zou[1,2,3] · Cuili Xiang[1,2,3] · Hailiang Chu[1,2,3] · Shujun Qiu[1,2,3] · Fen Xu[1,2,3] · Lixian Sun[1,2,3]

Received: 2 September 2016 / Accepted: 25 June 2017 / Published online: 6 July 2017

Abstract Series of *n*-octadecane/expanded graphite composite phase-change materials (PCMs) with different mass ratio were prepared using *n*-octadecane as PCMs, expanded graphite as multi-porous supporting matrix through vacuum impregnation method. Microstructure, crystallization properties, energy storage behavior, thermal cycling property and intelligent temperature-control performance of the composite PCMs were investigated. Results show that the composite PCMs have a good energy storage property. The melting enthalpy and crystallization enthalpy can reach 164.85 and 176.51 J g^{-1}, respectively. Furthermore, the good thermal conductivity of expanded graphite reduces the super-cooling degree of *n*-octadecane and endows the composite PCMs with fast thermal response rate and excellent thermal cycling stability. As a result, the phase-change temperatures and phase-change enthalpy almost have no change after 50 thermal-cooling cycles. The test of intelligent temperature-control performance shows that the electronic radiator filled with the composite PCMs possesses a high intelligent temperature-control performance, and its temperature can sustain in the range of 22–27.5 °C for about 6120 s. These results indicate that the prepared composite PCMs possess good comprehensive property and can be widely used in energy storage and thermal management systems.

Keywords Expanded graphite · *n*-octadecane · Composite phase-change materials · Thermal performance

✉ Huanzhi Zhang
zhanghuanzhi@guet.edu.cn

✉ Lixian Sun
sunlx@guet.edu.cn

[1] Department of Material Science and Engineering, Guilin University of Electronic Technology, Guilin 541004, People's Republic of China

[2] Guangxi Collaborative Innovation Center of Structure and Property for New Energy Materials, Guilin 541004, People's Republic of China

[3] Guangxi Key Laboratory of Information Materials, Guilin University of Electronic Technology, Guilin 541004, People's Republic of China

Introduction

Nowadays, the limited reserves of fossil fuels make the effective utilization of energy a general concern. Phase-change materials (PCMs) which are capacity of storing and releasing thermal energy during phase-change procedure provide an elegant and feasible solution to improve energy utilization in many sectors [1–3]. Furthermore, the application of PCMs for energy storage not only can reduce the mismatch between energy supply and demand, but also plays an important role in conserving energy and thermal management [2, 4, 5]. Recently, using PCMs has attracted increasing interests in thermal energy storage, as it can provide high energy storage density within small temperature intervals. Therefore, PCMs for thermal energy storage have been extensively employed in a wide of applications including usage of solar energy, energy-efficient building and thermal management of electronic devices.

Currently, during the different groups of PCMs, it is reported that paraffins, which are a kind of promising solid–liquid organic PCMs, possess high latent heat storage capacity over a narrow temperature range, non-toxicity, no super-cooling and precipitation phenomenon, high chemical and thermal stability and ecologically harmless [6]. Among various paraffin PCMs, *n*-octadecane has always been viewed as the most valuable one in practical applications due

to its suitable phase-change temperature (28.2 °C) and high latent heat storage capacity (245 J g^{-1}). In addition, *n*-octadecane possesses desirable characteristics including good chemical and thermal stability, less expensive, low vapor pressure, non-corrosiveness, low vapor pressure. However, the ubiquitous defects of seepage of the melting PCM during phase-change procedure and low thermal conductivity [0.35 W m^{-1} K^{-1} (s) and 0.149 W m^{-1} K^{-1} (l)] are the main factors that restrict its widely practical applications in thermal energy storage [7, 8].

In order to address these problems, researchers have focused on improving the shape-stabilization and thermal conductivity of *n*-octadecane as PCM. Encapsulation techniques provide opportunities to prevent leakage of the melting PCM. Moreover, encapsulation techniques can improve the thermal conductivity of PCMs with high heat transfer area, reduce reactivity with the outside environment and control volume changes during phase transition [2, 9]. Consequently, researchers focus on the preparation of shape-stabilized PCMs which contain solid–liquid PCM and supporting material by means of encapsulation [10–12]. At present, expanded graphite has attracted considerable attention to prepare form-stable composite PCMs due to its reticulated multi-porous structure. In addition, expanded graphite has good adsorption properties, high temperature resistance, high oxidation resistance, high corrosion resistance and great thermal conductivity [13, 14]. As a result, a large number of scholars have done much research about composite PCMs by using expanded graphite as a supporting material. However, thermal energy storage density and thermal repeatability of the composite PCMs still need to be improved [15, 16]. Besides, the thermal management effect of the composite PCMs is rarely investigated. Therefore, it is still important to ameliorate the thermal conductivity, thermal properties and practical application effect of the composite PCMs.

Hence, in the present study, series of *n*-octadecane/expanded graphite composite PCMs with different mass ratios were prepared using *n*-octadecane as PCM and expanded graphite as multi-porous supporting matrix through vacuum impregnation method. At the same time, this study also investigates the microstructure, thermal properties and intelligent temperature-control performance of the obtained composite PCMs.

Experimental

Materials

Flake graphite with an average particle size of 200 meshes and expansion ratio of 200 mL g^{-1} was purchased from Qingdao Graphite Co. Ltd. (Qingdao, China). *n*-Octadecane with a purity of 90% was obtained from Tianjin Alfa Aesar Co. (Tianjin, China).

Preparation of *n*-octadecane/expanded graphite composite PCMs

The *n*-octadecane/expanded graphite composite PCMs were prepared in two steps. First, flake graphite was put into a muffle furnace at 900 °C for 60 s forming vermicular expanded graphite. Next, *n*-octadecane/expanded graphite composite PCMs were prepared using a vacuum impregnation method. *n*-Octadecane was placed in a beaker and heated to melt at 50 °C in a vacuum drying oven. Then, some expanded graphite was added in the beaker and well mixed with melting *n*-octadecane by stirring. After that, the mixture was heated in a vacuum drying oven at 50 °C for 2 h. At last, series of *n*-octadecane/expanded graphite composite PCMs with different mass ratios were prepared. The mass ratios of *n*-octadecane/expanded graphite are 6:4, 7:3, 8:2, 9:1, and the corresponding sample is marked as PCM1, PCM2, PCM3, PCM4, respectively.

Characterization

Fourier transform-infrared spectroscopy (FT-IR) spectra were recorded on an Equinox 55 FT-IR spectrometer (Bruker, Germany) using KBr pellet in the wave number range of 4000–400 cm^{-1}. The crystalline structures of expanded graphite and the composite PCMs were investigated by X-ray diffraction (XRD, Bruker-D8 Advance, Germany), operating at 40 kV and 40 mA with a 2θ scanning range of 20°–80° in a step of 0.02°. Scanning electron microscopy (SEM) images of the composite PCMs were obtained from a JSM-6360LV microscope, operating at an accelerating voltage of 20 kV. The samples were coated with gold–palladium alloy prior to SEM analysis. The microstructures of expanded graphite and the composite PCM were detected by transmission electron microscopy (TEM, Hitachi JEM-1200EX, JEOL Ltd., Japan) operating at an acceleration voltage of 120 kV. The sample was dispersed in ethanol, and some pieces were collected on carbon-coated 300-mesh copper grids for the TEM observation. The melting and crystallization behaviors of the composite PCMs were measured by differential scanning calorimeter (DSC, Setaram, Sensys), and the test was carried out from −30 to 60 °C with a heating rate of 5 °C min^{-1} in nitrogen atmosphere. The masses of the composites were about 5–10 mg. The temperature scale was calibrated using high purity indium, tin and lead. In most cases, the transition temperatures were reproducible to within 0.5 °C. Thermal cycling stability of the composite PCMs was carried out consecutively up to 50

thermal cycles using the DSC calorimeter. Thermal stability of the prepared composite PCMs after thermal cycling test was characterized via thermogravimetric analysis (TG, TA-SDT Q600, American) from room temperature to 600 °C at a heating rate of 10 °C min^{-1} under nitrogen atmosphere with a flowing rate of 100 mL min^{-1}. The intelligent temperature-control performance of the composite PCMs was investigated by using multi-channels data acquisition equipment (Shenzhen Kai-LiDi Technology CO. LTD.). The measurement was taken by using an electronic radiator which is a tank radiator made of aluminum. First, the channels of the radiator were fully filled with the prepared composite PCMs. Then, a thermocouple was inserted into the middle position of the channel in the radiator. And the thermocouple was connected with the multi-channels data acquisition equipment. At last, the electronic radiator was irradiated with a 275 W infrared lamp and the corresponding temperature changes were collected by the data acquisition equipment.

Results and discussion

Chemical structure of the composite PCMs

Chemical structures of the composite PCMs synthesized with different *n*-octadecane/expanded graphite mass ratios were characterized by FT-IR spectroscopy. The resulting spectra are illustrated in Fig. 1. The FT-IR spectrum of expanded graphite shows the characteristic absorption peaks at 1645 and 3450 cm^{-1}, corresponding to the stretching vibrations of C=O and –OH, respectively. All the *n*-octadecane/expanded graphite composite PCMs also exhibit characteristic peaks at the same positions as those observed from FT-IR spectrum of expanded graphite. At the same time, the composite PCMs exhibit characteristic absorption peaks at 2800 and 2900 cm^{-1} caused by typical asymmetric and symmetric stretching vibration of $–CH_3$. The absorption peaks at approximately 1454 cm^{-1} belong to the bending deformation of $–CH_3$ and $–CH_2–$, whereas the peak at 717 cm^{-1} is due to the in-plane rocking vibration of $–CH_3$ [17]. These absorption peaks attach to the characteristic peaks of *n*-octadecane. It indicates that the composite PCMs were successfully prepared by using *n*-octadecane as PCM and expanded graphite as supporting material. It is clear that there was no strong chemical interaction between *n*-octadecane and expanded graphite, and the composite PCMs were physical mixtures. These results imply that the *n*-octadecane was successfully filled into the porous structure of expanded graphite, and thus, seepage of the molten *n*-octadecane from the porous structure was prevented.

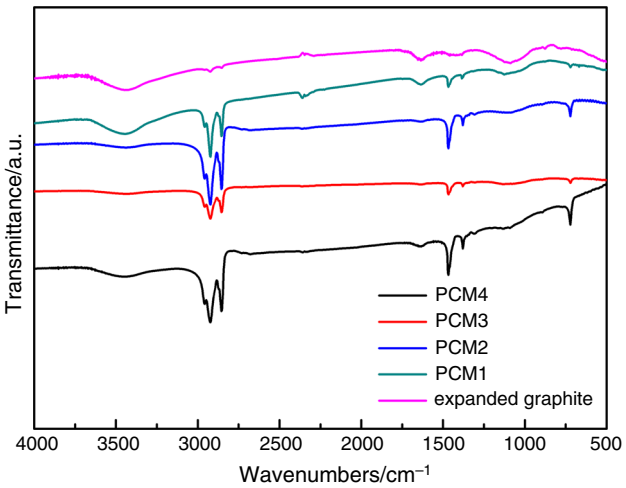

Fig. 1 FT-IR spectra of the composite PCMs with different *n*-octadecane/expanded graphite mass ratios

Morphologies of the composite PCMs

The SEM images of expanded graphite and the *n*-octadecane/expanded graphite composite PCMs with different ratios are presented in Fig. 2. As shown in Fig. 2a, expanded graphite consists of overlapped graphite flakes and has a multilayered structure, forming abundant crevice-like and net-like pores. Owing to this porous structure, *n*-octadecane can be adsorbed and filled into expanded graphite. It can be seen from Fig. 2b–e that *n*-octadecane was well mixed into expanded graphite matrix and adsorbed into the porous structure and surface of expanded graphite by capillary forces and surface tension between *n*-octadecane and expanded graphite. Besides, as the content of *n*-octadecane in the composites increases, the surface of expanded graphite becomes smooth and compact. However, as the mass ratio of *n*-octadecane/expanded graphite increases to 9:1, a large amount of *n*-octadecane is found on the surface of expanded graphite (seen from Fig. 2e), which will lead to the leakage of molten *n*-octadecane during phase-change procedure. While the mass ratio of *n*-octadecane/expanded graphite is 8:2, the sample shows a quite compact structure as observed from Fig. 2d. It indicates that the porous structure of expanded graphite was adequately filled and wrapped by 80 mass% *n*-octadecane which is enough to homogeneously occupy the pores and surface of expanded graphite resulting in the smooth surface. And expanded graphite can keep them from leakage during phase-change procedure. Once the content of *n*-octadecane increases, there will be redundant *n*-octadecane accumulating on the surface of the composites. This result suggests that 8:2 may be the optimum ratio to prepare the *n*-octadecane/expanded graphite composite PCMs with good thermal properties.

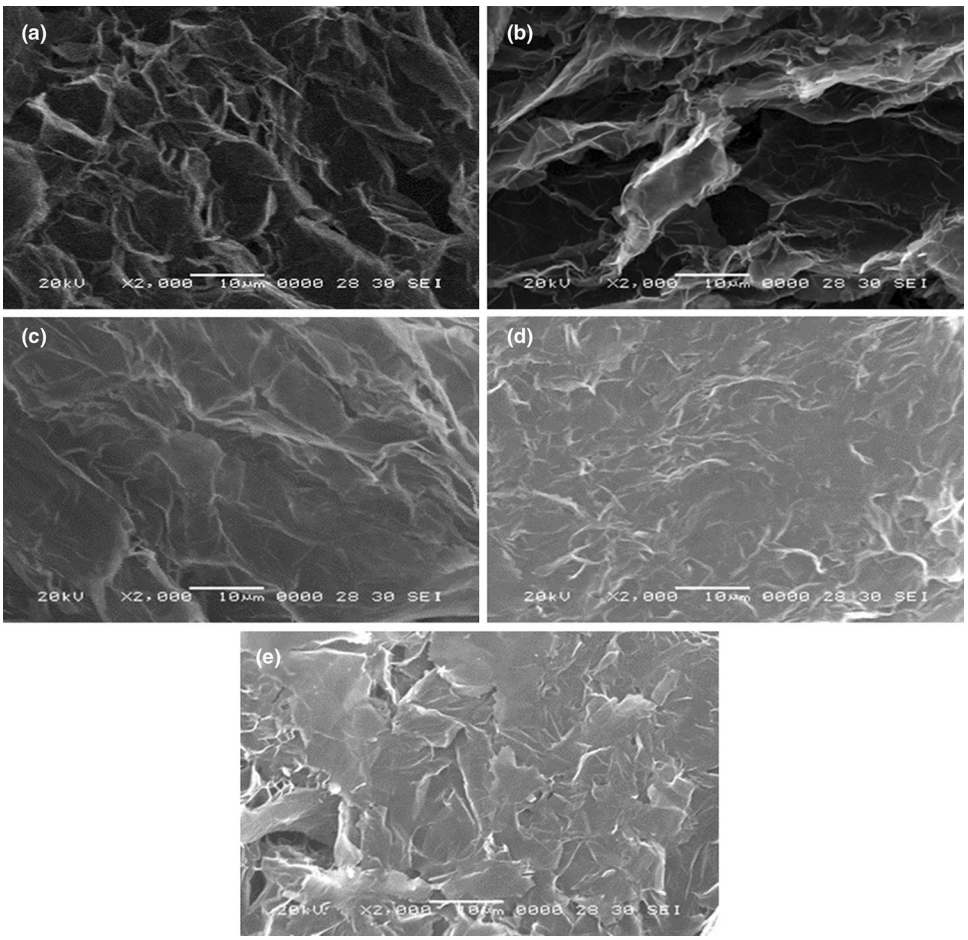

Fig. 2 SEM images of **a** the synthesized expanded graphite; and the composite PCMs: **b** PCM1, **c** PCM2, **d** PCM3, **e** PCM4

Furthermore, in order to further investigated the microstructure of the composite PCMs, TEM photographs of expanded graphite and the composite PCM with 8:2 *n*-octadecane/expanded graphite mass ratio were carried out and are shown in Fig. 3. As represented in Fig. 3a, the prepared expanded graphite has flat and semitransparent slices with some wrinkles and folds. It can be observed from Fig. 3b that the composite PCM exhibits a non-transparent structure which suggests that *n*-octadecane was successfully filled into the porous structure of expanded graphite by capillary forces and surface tension between *n*-octadecane and expanded graphite. These results are consistent with those obtained from the SEM images and FT-IR spectrum.

Crystallization properties of the composite PCMs

XRD patterns are used to reveal the crystallization properties of the prepared expanded graphite and composite PCMs, which are shown in Fig. 4. It is obviously found that the XRD pattern of the expanded graphite has one strong diffraction peak centered at 26.2° due to the feature peak (002) of graphite, and this peak also appears in the patterns of all composite PCMs. In addition, the peaks appearing at 11.7°, 19.5°, 19.9°, 22.4°, 23.7°, 24.8°, 34.8°, 39.7° and 44.5° of the composite PCMs are caused by the crystalline structure of *n*-octadecane. Besides, the intensity of these peaks enhances with the increase in *n*-octadecane/expanded graphite mass ratio. These results indicated that the crystal structure of *n*-octadecane in the composite PCMs is not changed implying that *n*-octadecane was absorbed into the porous structure of expanded graphite by physical interaction without chemical reaction.

Thermal properties of the composite PCMs

The phase-change behaviors of the *n*-octadecane/expanded graphite composite PCMs were investigated by DSC. Figure 5 presents the heating and cooling curves of the composite PCMs, where the upward peak indicates the endothermic process while the downward corresponds to the exothermic one. The melting and crystallization

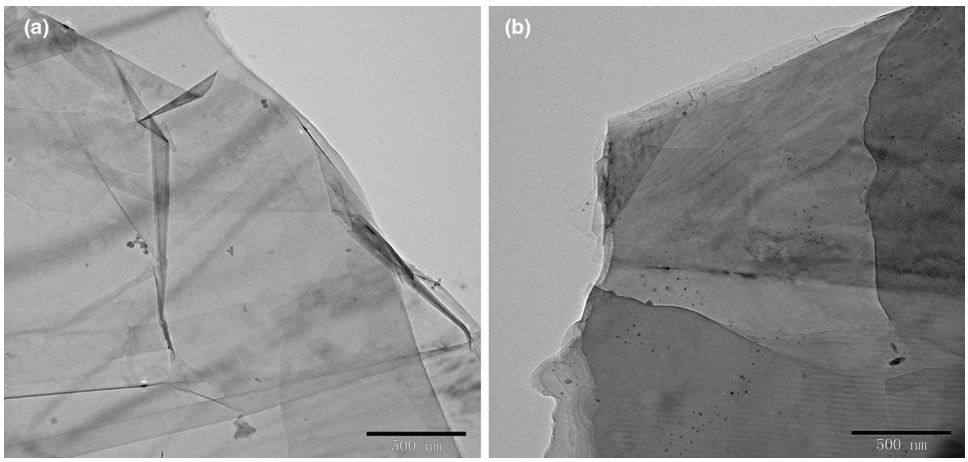

Fig. 3 TEM images of **a** the synthesized expanded graphite and **b** PCM3

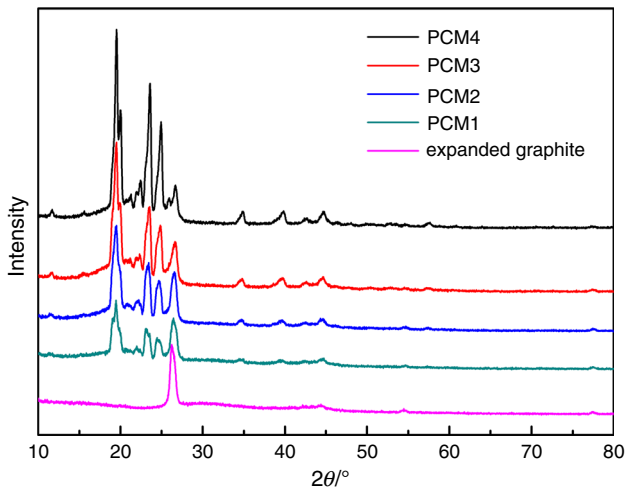

Fig. 4 XRD patterns of the prepared expanded graphite and composite PCMs

parameters of all the samples obtained from DSC analysis are listed in Table 1. As seen from Fig. 5, a single and well-resolved endothermic peak can be significantly observed for all the samples on the DSC heating and cooling curves. Besides, area of the corresponding peak enlarges with the increase in *n*-octadecane/expanded graphite mass ratio. These results show that the porous structure of expanded graphite has no effect on the phase-change behavior of the interior *n*-octadecane, and all the *n*-octadecane/expanded graphite composite PCMs possess high phase-change energy storage property.

Moreover, as shown in Table 1, it is evident that the mass ratio of *n*-octadecane has a significant influence on the thermal properties of the composite PCMs. Obviously, the melting temperature of the samples decreases with the increase in expanded graphite content. It indicates that the good thermal conductivity of the expanded graphite

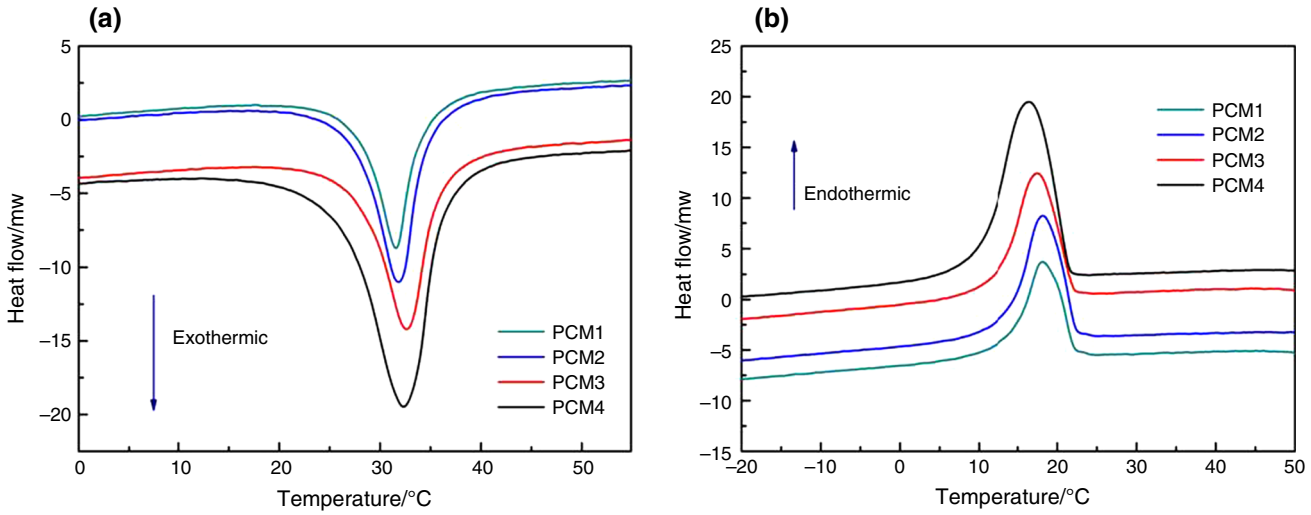

Fig. 5 DSC curves of the *n*-octadecane/expanded graphite composite PCMs: **a** exothermic curves; **b** endothermic curves. The numbers of the *curves* are corresponding to the sample codes in Table 1

Table 1 Thermal properties of the composite PCMs with different *n*-octadecane/expanded graphite mass ratios

Sample code	Melting temperature/ °C	Melting enthalpy/J g^{-1}	Crystallization temperature/ °C	Crystallization enthalpy/J g^{-1}
PCM1	31.562	127.052	18.133	−144.263
PCM2	31.864	147.236	18.161	−154.253
PCM3	32.650	164.854	17.412	−176.512
PCM4	32.337	176.358	16.394	−191.307

accelerates the melting behavior of *n*-octadecane. The same result can also be seen in the freezing process. The crystallization temperature of the samples increases with the increase in expanded graphite content. These results mean that *n*-octadecane was homogeneously dispersed in the porous structure of expanded graphite and expanded graphite looks like a three dimensional thermal conductive network for the interior *n*-octadecane. Hence, the interior *n*-octadecane can respond quickly to the temperature variations resulting in the decrease in melting temperature and the increase in crystal temperature. Furthermore, the good thermal response rate of the composite PCMs also reduces the super-cooling degree of *n*-octadecane and may endow the composite PCMs with excellent thermal cycling stability. These results further confirm that *n*-octadecane was effectively absorbed into the porous structure of expanded graphite which also entrust the interior *n*-octadecane with good comprehensive properties.

In addition, all the obtained composite PCMs possess high latent heat which increases with the increase in *n*-octadecane content. As the sample with 80 mass% *n*-octadecane, its melting enthalpy and crystallization enthalpy are 164.85 and 176.51 J g^{-1}, respectively. And the latent heat of the sample incorporated with 90 mass% *n*-octadecane is the highest among all the samples. Nevertheless, we have learnt from the SEM results that there is excessive *n*-octadecane attaching to the surface of the sample which may lead to the leakage of molten *n*-octadecane during phase-change procedure. In summary, all the results demonstrate the composite PCMs incorporated with 80 mass% *n*-octadecane possess good comprehensive property which can be widely used in energy storage and thermal management systems.

Thermal cycling stability of the composite PCMs

Thermal cycling test was performed to determine the thermal reliability and endurance property of the composite PCMs. They were evaluated in terms of variations in phase-change temperatures and latent heat values after 50 thermal cycles. From the above results, we can determine that the *n*-octadecane/expanded graphite composite PCM with the mass ratio of 8:2 possesses good phase-change behavior. Therefore, the thermal cycling test was conducted on this sample. The obtained DSC curves and the corresponding latent heat from DSC analysis of the sample for 50 thermal cycles are presented in Fig. 6a, b, respectively. It can be clearly seen that the phase-change temperatures and the latent heats of the composite PCM almost remain the same, which prove that the composite PCM possesses excellent thermal cycling stability. Moreover, the FT-IR spectra and TG curves of the sample before and after 50 thermal cycles are shown in Fig. 6c, d, respectively. From Fig. 6(c), no characteristic peak disappears or has a location shift and no new characteristic peak emerges after 50 thermal cycles, which further illustrate that the composite PCM possesses commendable thermal reliability. Moreover, as shown in Fig. 6d, it can be clearly observed that the TG curves of the sample almost keep no significant change for 50 DSC thermal cycles. It also indicates that the composite PCMs possess good thermal cycling stability. Therefore, the prepared *n*-octadecane/expanded graphite composite PCMs not only have an excellent phase-change behavior but also possess good thermal cycling stability, meaning that they have a great potential in applications of energy storage and thermal management.

Intelligent temperature-control properties of the composite PCMs

Figure 7 presents the intelligent temperature-control performance results of the composite PCMs. It is significant that the temperature rising rate of the electronic radiator is faster than that of the electronic radiator filled with PCMs in the whole heating period. And the temperature of the electronic radiator increases with the extension of radiation time. However, the temperature of the electronic radiator filled with PCMs is just increasing at the initial heating stage. Then, its temperature begins to increase slowly at around 22 °C and it needs 6120 s to increase to 27.5 °C; hence, there is an approximately constant temperature platform in the temperature variation curve in Fig. 7. This result implies that the composite PCMs filled in the electronic radiator absorb the radiant heat of the infrared lamp because of their phase change during the heating process. Consequently, the temperature of the electronic radiator filled with PCMs is controlled in the range of 22–27.5 °C

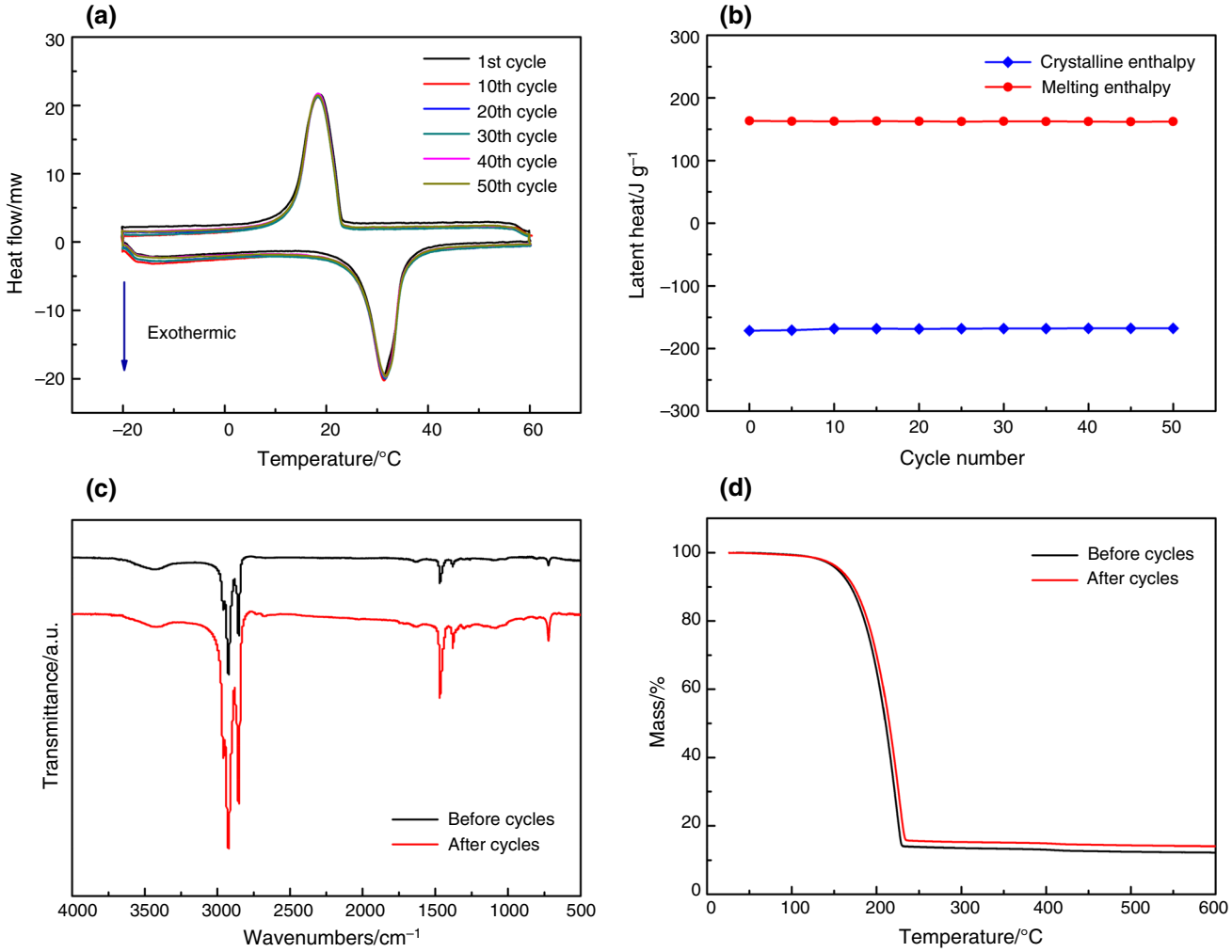

Fig. 6 **a** DSC curves and **b** latent heats of PCM3 for 50 thermal cycles; **c** FT-IR spectra and **d** TG curves of PCM3 before and after thermal cycling test

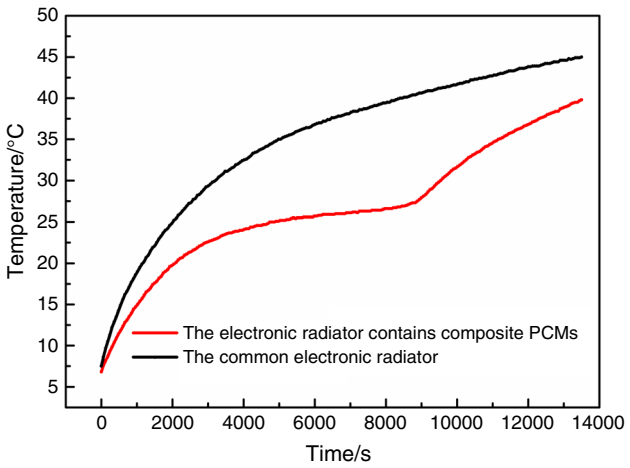

Fig. 7 Temperature variation curves versus time for the composite PCMs

for about 6120 s. Meanwhile, it takes only 1020 s for the electronic radiator without composite PCMs increasing from 22 to 27.5 °C. These results indicate that the electronic radiator filled with PCMs has an excellent intelligent temperature-control property which further shows that the composite PCMs prepared in this study has a broad application prospect in fields of thermal energy storage and thermal management.

Conclusions

Series of *n*-octadecane/expanded graphite composite PCMs with different mass ratios were prepared through vacuum impregnation method. FT-IR spectra confirm that there was no strong chemical interaction between *n*-octadecane and expanded graphite, and *n*-octadecane was successfully

filled into the porous structure of expanded graphite. The morphology investigation suggests that the optimum mass ratio of *n*-octadecane/the expanded graphite is 8:2 to prepare composite PCMs. Furthermore, this sample has a much better phase-change properties, and its melting enthalpy and crystallization enthalpy can reach 164.85 and 176.51 J g^{-1}, respectively. Moreover, the composite material has excellent thermal cycling stability and its phase-change enthalpy almost has no change after 50 times of DSC heating and cooling. In addition, the composite PCMs possess high intelligent temperature-control performance, which can control the temperature of an electronic radiator sustaining in the range of 22–27.5 °C for about 6120 s. All these results demonstrate that the obtained composite PCMs incorporated with 80 mass% *n*-octadecane possess good comprehensive property which can be widely used in energy storage and thermal management systems.

Acknowledgements The authors greatly appreciate the financial support by the National Natural Science Foundation of China (Grant Nos. 51102230, 51462006), the Guangxi Natural Science Foundation (Nos. 2014GXNSFAA118401, 2013GXNSFBA019244), and Program for Postgraduate Joint Training Base of GUET-CJYRE (No. 20160513-14-Z).

References

1. Liu LK, Su D, Tang YJ, Fang GY. Thermal conductivity enhancement of phase change materials for thermal energy storage: a review. Renew Sustain Energy Rev. 2016;62:305–17.
2. Pielichowska K, Pielichowski K. Phase change materials for thermal energy storage. Prog Mater Sci. 2014;65:67–123.
3. Xu B, Li PW, Chan C. Application of phase change materials for thermal energy storage in concentrated solar thermal power plants: a review to recent developments. Appl Energy. 2015;160:286–307.
4. Meng X, Zhang HZ, Sun LX, Xu F, Jiao QZ, Zhao ZM, Zhang J, Zhou HY, Yutaka S, Liu YL. Preparation and thermal properties of fatty acids/CNTs composite as shape-stabilized phase change materials. J Therm Anal Calorim. 2013;111:377–84.
5. Tyagi VV, Pandey AK, Kaushik SC, Tyagi SK. Thermal performance evaluation of a solar air heater with and without thermal energy storage. J Therm Anal Calorim. 2012;107:1345–52.
6. Giro-Paloma J, Martínez M, Cabeza LF, Fernández AI. Types, methods, techniques, and applications for microencapsulated phase change materials (MPCM): a review. Renew Sustainable Energy Rev. 2016;53:1059–75.
7. Khadiran T, Hussein MZ, Zainal Z, Rusli R. Encapsulation techniques for organic phase change materials as thermal energy storage medium: a review. Sol Energ Mat Sol C. 2015;143:78–98.
8. Su WG, Darkwa J, Kokogiannakis G. Review of solid–liquid phase change materials and their encapsulation technologies. Renew Sustain Energy Rev. 2015;48:373–91.
9. Jurkowska M, Szczygieł I. Review on properties of microencapsulated phase change materials slurries (mPCMS). Appl Therm Eng. 2016;98:365–73.
10. Zhang Y, Wang XD, Wu DZ. Design and fabrication of dual-functional microcapsules containing phase change material core and zirconium oxide shell with fluorescent characteristics. Sol Energy Mater Sol Cells. 2015;133:56–68.
11. Zhu YL, Liang SE, Wang H, Zhang K, Jia XR, Tian CR, Zhou YL, Wang JH. Morphological control and thermal properties of nanoencapsulated *n*-octadecane phase change material with organosilica shell materials. Energy Convers Manag. 2016;119:151–62.
12. Zhang HZ, Sun SY, Wang XD, Wu DZ. Fabrication of microencapsulated phase change materials based on *n*-octadecane core and silica shell through interfacial polycondensation. Colloids Surf A. 2011;389:104–17.
13. Haghighi AH, Sheydaei M, Allahbakhsh A, Ghatarband M, Hosseini FS. Thermal performance of poly(ethylene disulfide)/expanded graphite nanocomposites. J Therm Anal Calorim. 2014;117:525–35.
14. Karkri M, Lachheb M, Gossard D, Ben Nasrallah S, AlMaadeed MA. Improvement of thermal conductivity of paraffin by adding expanded graphite. J Compos Mater. 2016;50:2589–601.
15. Duan ZJ, Zhang HZ, Sun LX, Cao Z, Xu F, Zou YJ, Chu HL, Qiu SJ, Xiang CL, Zhou HY. CaCl2·6H2O/Expanded graphite composite as form-stable phase change materials for thermal energy storage. J Therm Anal Calorim. 2014;115:111–7.
16. Zhang H, Gao XN, Chen CX, Xu T, Fang YT, Zhang ZG. A capric–palmitic–stearic acid ternary eutectic mixture/expanded graphite composite phase change material for thermal energy storage. Compos A. 2016;87:138–45.
17. Kim D, Jung J, Kim Y, Lee M, Seo J, Khan SB. Structure and thermal properties of octadecane/expanded graphite composites as shape-stabilized phase change materials. Int J Heat Mass Transf. 2016;95:735–41.